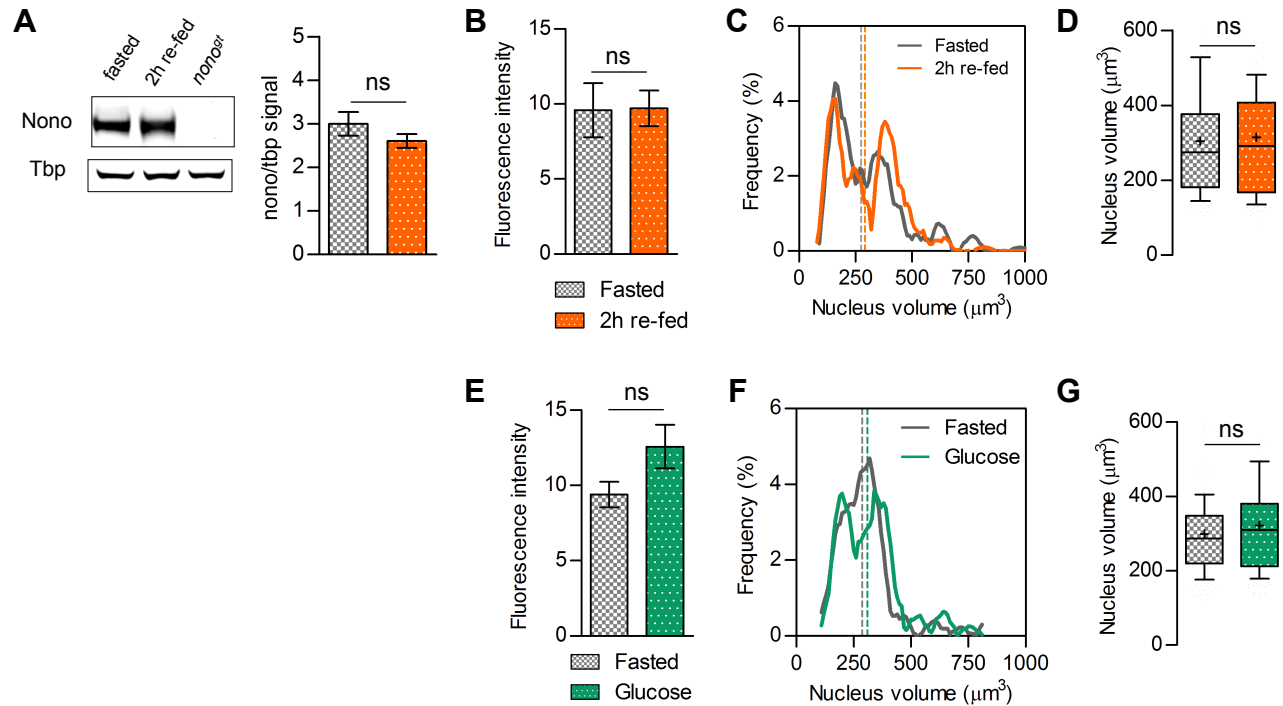


# Figure S1



**Figure S1. NONO protein abundance in the nucleus and liver nuclei size are unchanged upon feeding. Related to figure 1.**

A) Representative western blot of NONO expression,  $n=5$ . (B) and (E) Average NONO fluorescence intensity in the liver nucleus normalised to background; (C) and (F) distribution of the liver cell nucleus volume; (D) and (G) average liver cell nucleus volume; (C), (D), (F), and (G)  $n>170$  nuclei; (B) and (E)  $n=12$  images per group; For (D) and (G) results are represented as box and whiskers: 10-90 percentile range, '+' sign represents mean. For (A), (B) and (E) results are represented as  $\text{mean} \pm \text{SEM}$ . Statistical analysis student t test.

# Figure S2

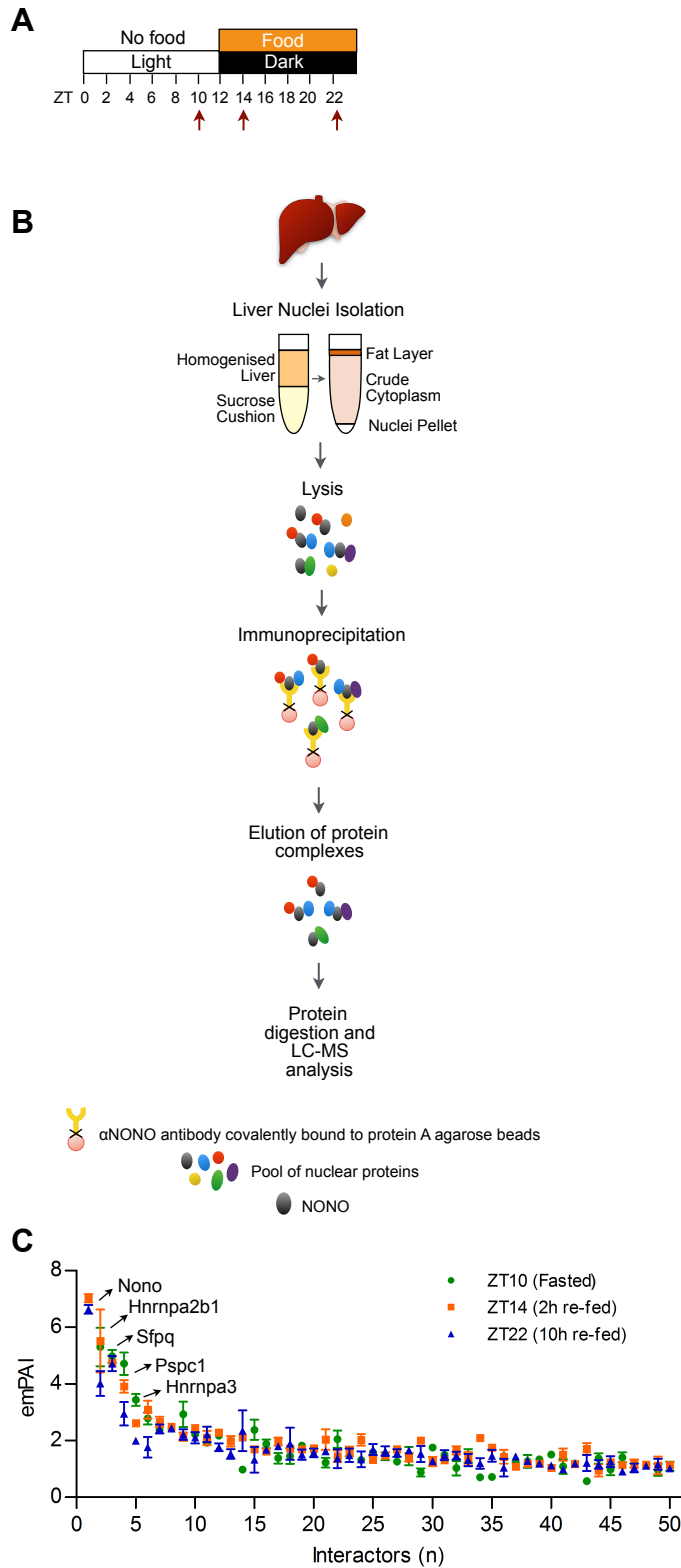


**Figure S2. Characterization of NONO interactors by IP-MS. Related to Table 1 and STAR methods.**

(A) Experimental scheme indicating the time points at which liver were collected for IP-mass spectrometry analysis. Livers were collected at the end of the fasting phase (ZT10), 2h after the start of the feeding phase (ZT14) and at the end of the feeding phase (ZT22). (B) Outline of the experimental methods for the NONO IP-MS in liver nuclei (see also STAR METHODS). Liver was homogenized and ultracentrifuged on a sucrose cushion to isolate liver nuclei. Nuclear lysates were incubated with agarose beads cross-linked to anti-NONO antibody. NONO and NONO interactors were eluted and identified by mass spectrometry. (C) 50 most abundant NONO interactors sorted by average emPAI value. N=3 per group. Data are represented as mean±SEM. (D) Main classes of NONO interactors. With (\*) are indicated proteins that were previously identified in paraspeckles or interacting with NONO (Close et al., 2012; Fong et al., 2013; Naganuma et al., 2012; Salton et al., 2010; Tenzer et al., 2013; Zhang and Carmichael, 2001). See also Table S1.

Figure S3

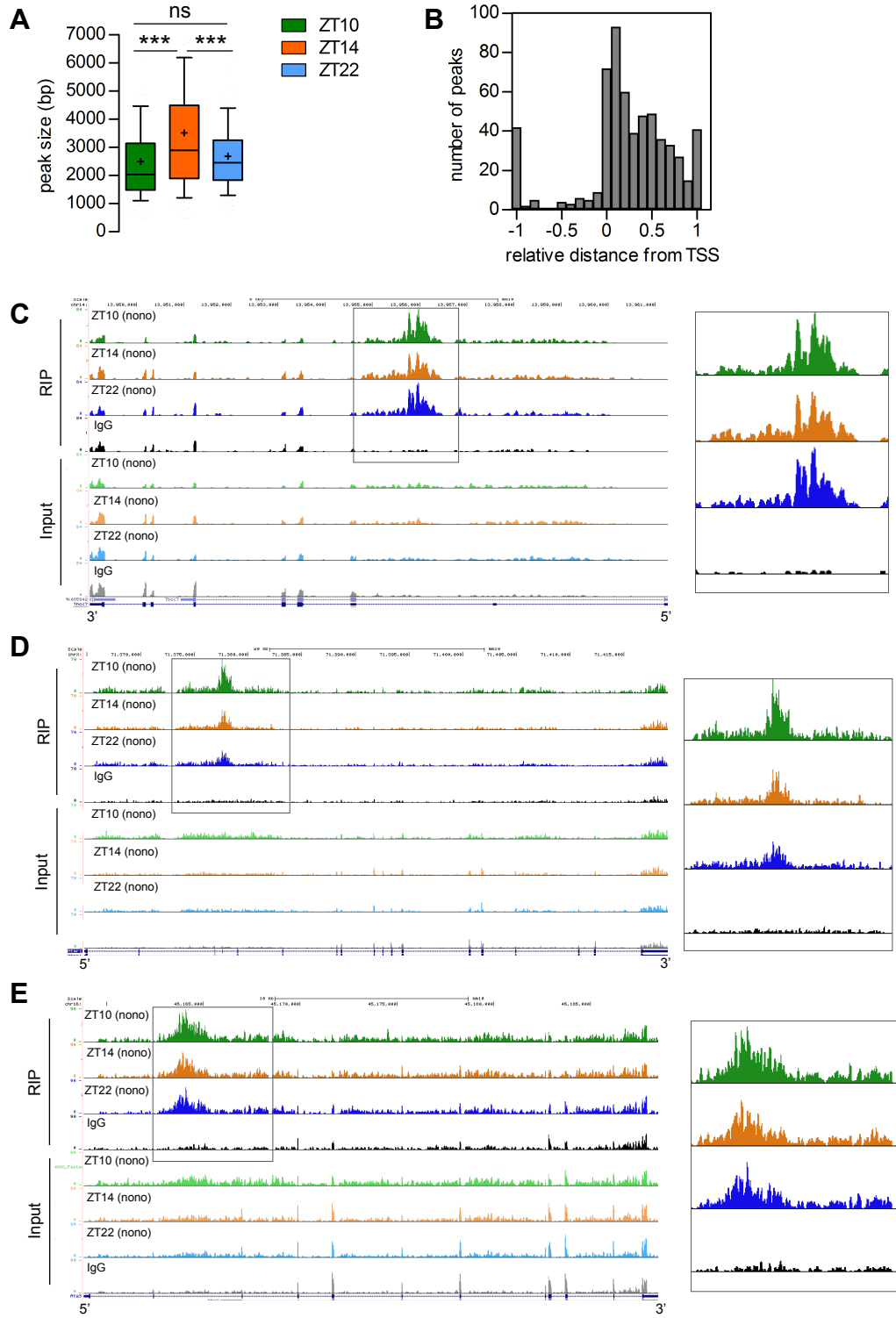


**Figure S3. NONO binds promoter-proximal introns and its binding activity increases upon feeding. Related to Figure 2.**

(A) Average RIP-seq peak size for the 134 common targets at each indicated time point. (B) Relative distance of NONO RIP-seq peaks (ZT14) from the TSS normalized to gene size. (C), (D) and (E) UCSC genome browser view of the RIP-seq reads mapping to Thoc7 (C), Mtmr1 (D) and Atg3 (E) genes, the right panels highlight the NONO RIP-seq peaks in Thoc7 intron 1, and Mtmr1 intron 2 and Atg3 intron 2. Each time point is a pool of 2 independent RIP experiments. In (A) results are represented as box and whiskers: 10-90 percentile range, '+' sign represents mean. Statistical analysis one-way ANOVA, \*\*\* $p < 0.0001$ .

**Figure S4**

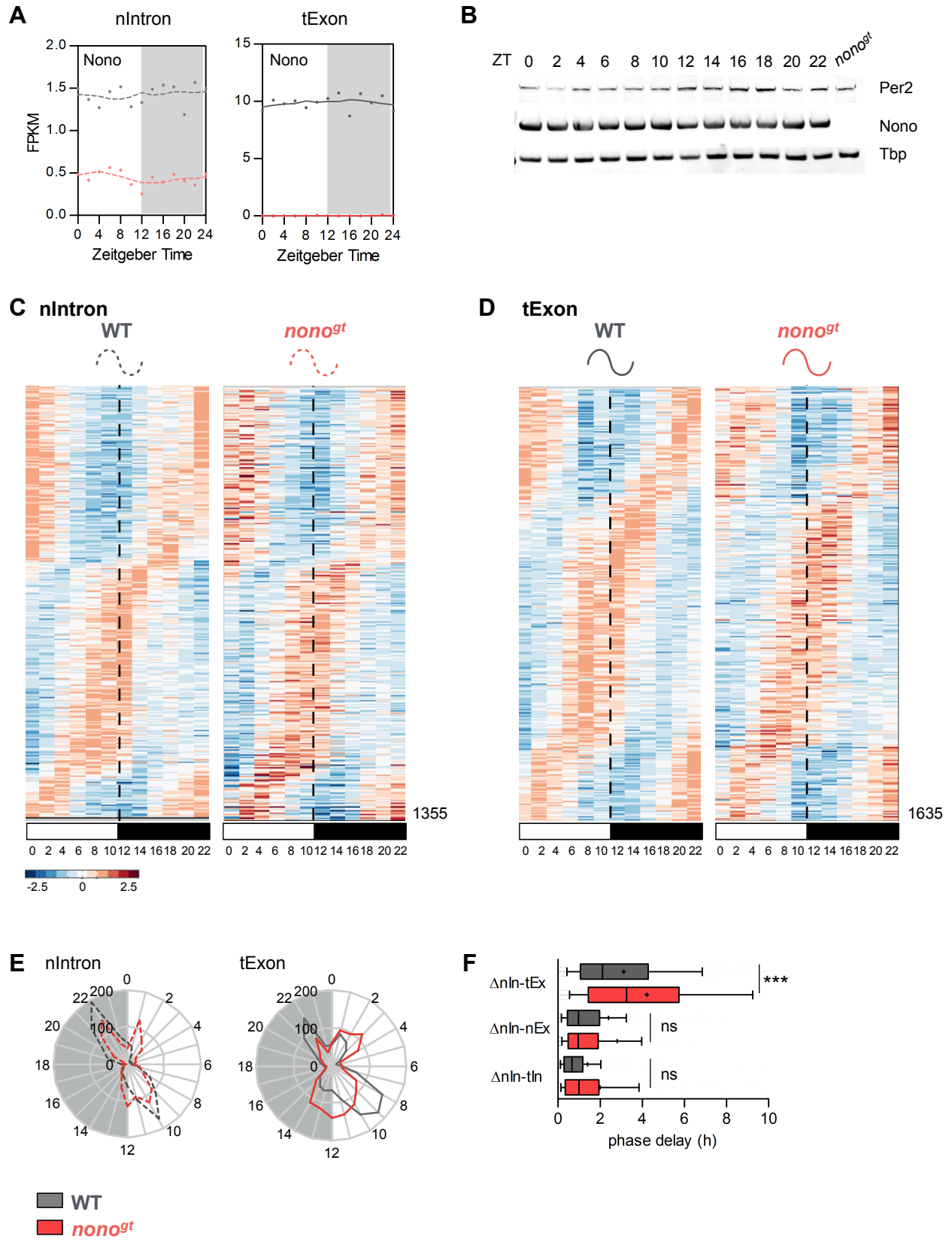


**Figure S4. Mature mRNA peak phase of expression is delayed in *nono<sup>gt</sup>* mice at genome wide level. Related to Figure 3.**

(A) Nono mRNA expression (FPKM) at the transcription level (nIntron) and at the mature mRNA level (tExon) across a 24 h cycle, samples were collected every 2 h starting at ZT0. Each time point is a pool of 2 mice. (B) NONO, PER2 and TBP protein expression in liver nuclei across a 24 h cycle, samples were collected every 2 h starting at ZT0. (C) Normalized profile of expression of genes cycling at the pre-mRNA level (nIntron) in both WT and *nono<sup>gt</sup>* mice at the indicated time points. (D) Normalized profile of expression of genes cycling at the mature mRNA level (tExon) in both WT and *nono<sup>gt</sup>* mice at the indicated time points. High expression is displayed in orange, low expression in blue. (E) Peak phase distribution of the same genes as in (C) and (D) separated by bins of 1h: left panel pre-mRNA peak phases (nIntron, n=1355), right panel mature mRNA peak phases (tExon, n=1635). (F) Phase delay between nIntrons and tExon, nIntron and nExon, nIntron and tIntron in WT and *nono<sup>gt</sup>* livers. Only genes with a positive delay (phase difference $\geq$ 0) were considered for this analysis. Statistical analysis one-way ANOVA, \*\*\*p<0,0001.

Figure S5

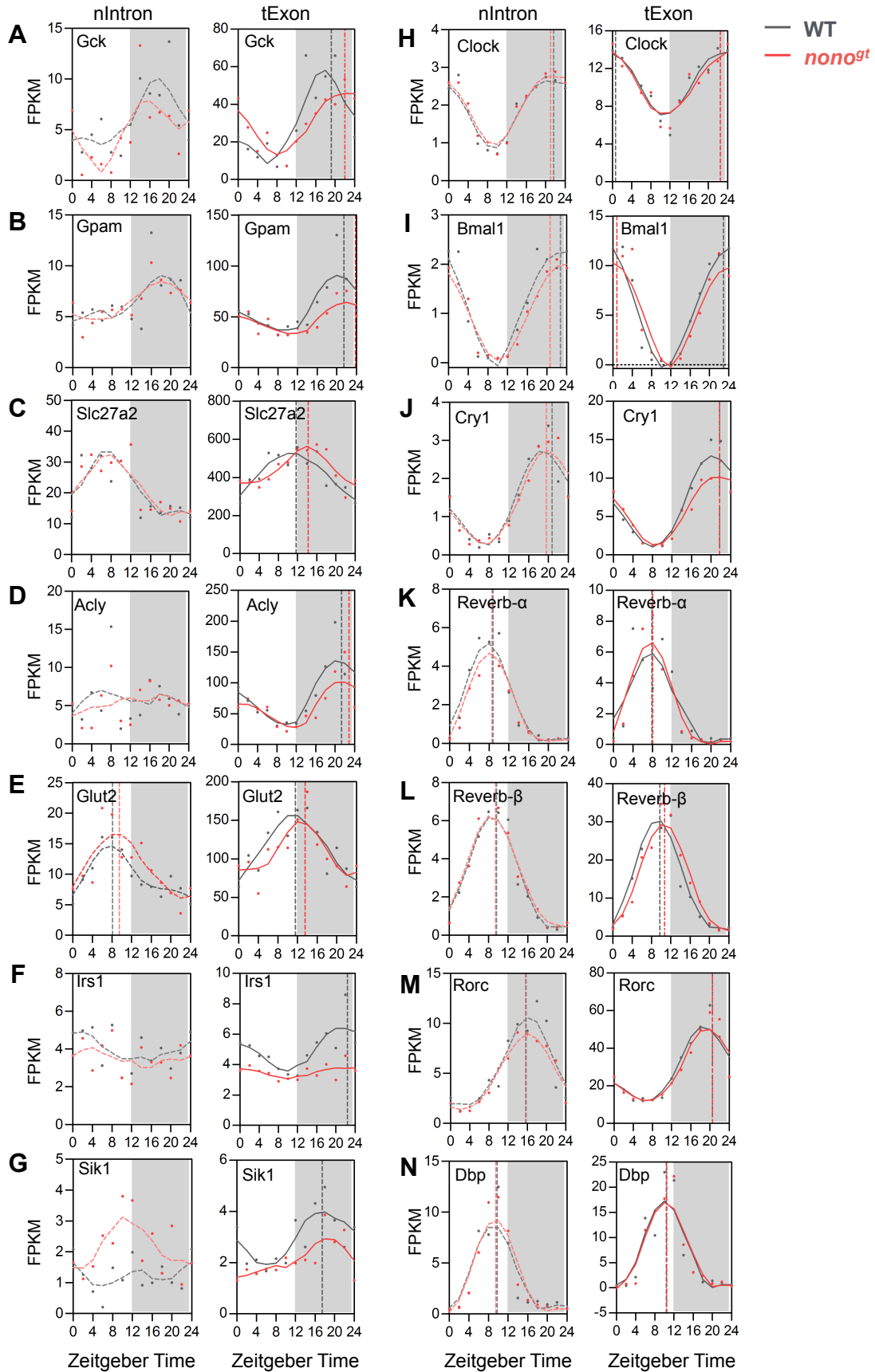




**Figure S5. Examples of transcription and mature mRNA rhythms in WT and *nono<sup>gt</sup>* livers.**

**Related to Figure 3**

Examples of gene expression at the transcription level (nIntron) and at the mature mRNA level (tExon) in the mouse liver, samples were collected every 2h starting at ZT0. When a gene is considered cycling its peak phase of expression calculated using metacycle (see STAR METHODS for details) is indicated as a dashed line. Each time point is a pool of 2 mice. (A-D) Examples of genes that are bound by NONO in the RIP-seq dataset and are rhythmic at the mRNA level but not at the transcription level in both genotypes. These genes are delayed in their phase of oscillation in *nono<sup>gt</sup>* livers. Phase delay: 2.9h (Gck), 2.3h (Gpam), 2.5h (Slc27a2), 1.6h (Acly). (E) Example of a gene that is bound by NONO in the RIP-seq dataset and is rhythmic both at the transcription and mRNA level in both genotypes. For this group of genes *nono<sup>gt</sup>* liver have a longer delay in the mRNA phase compared to the transcription phase. Glut2 gene phase delay: 1.4h (nIntron), 2h (tExon). (F-G) Examples of genes that are bound by NONO in the RIP-seq dataset, are not rhythmic at the transcription level and are rhythmic at the mRNA level only in the WT mice (loss of mRNA rhythmicity in *nono<sup>gt</sup>* mice). (H-N) Examples of clock genes profile of expression.

**Figure S6**

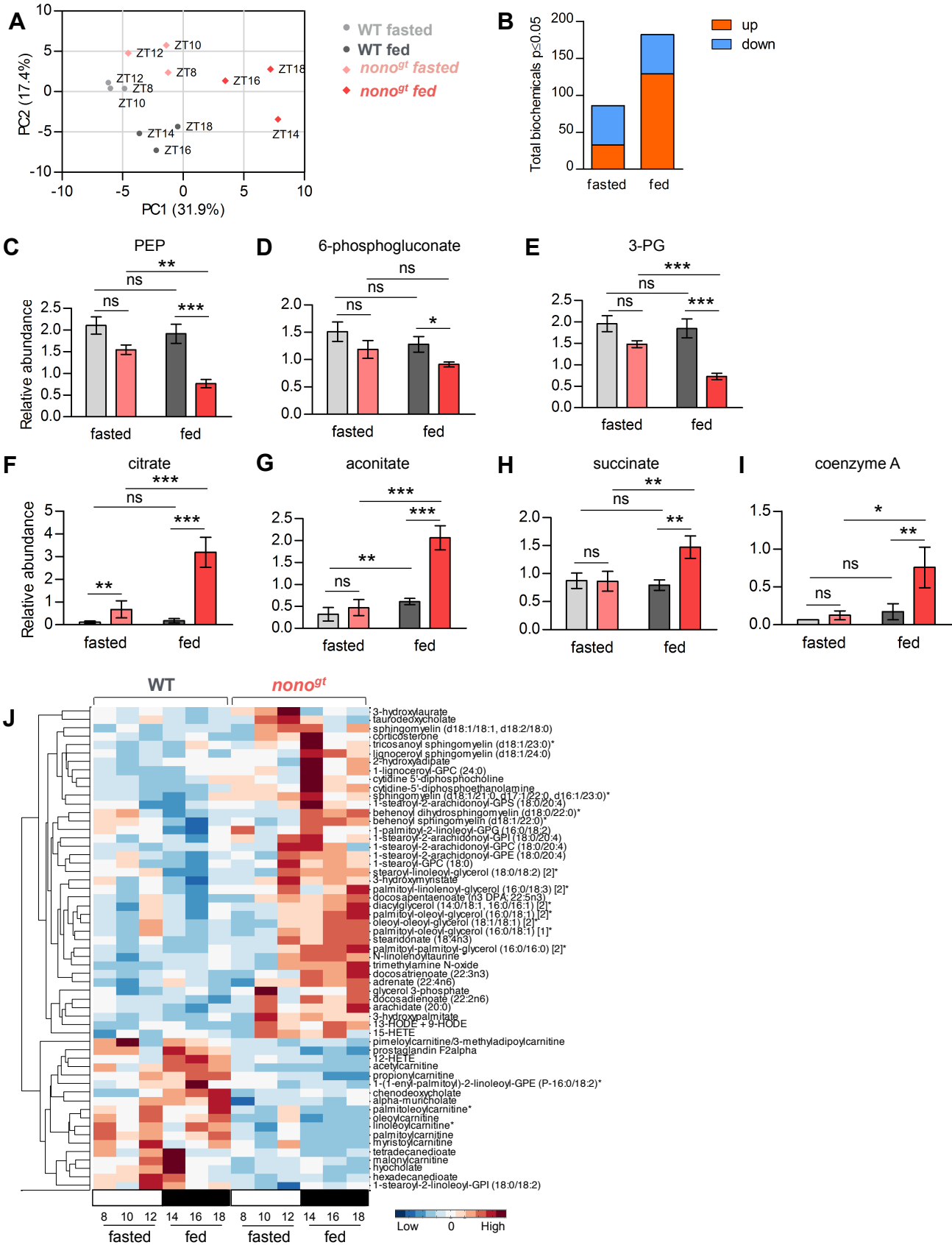


**Figure S6. Upon feeding several metabolites involved in glucose metabolism, lipid metabolism and the TCA cycle are changed in *nono<sup>gt</sup>* livers. Related to Figure 6.**

(A) PCA analysis of the metabolomics profile of WT and *nono<sup>gt</sup>* mice in fasted and re-fed conditions. (B) Number of significantly up and down-regulated metabolites in *nono<sup>gt</sup>* mice compared to *wt* in fasted and re-fed conditions. (C-I) Relative abundance (median normalized) of selected liver metabolites involved in glycolysis (C-E) and the TCA cycle (F-I). (J) Normalized quantification of lipid metabolites significantly altered between *wt* and *nono<sup>gt</sup>* mice. For metabolomics analysis liver samples were collected at 3 and 4 different time points respectively, fasted: ZT8, ZT10, ZT12; fed: ZT14, ZT16, ZT18, ZT20 (2 mice per time point). Statistical analyses were performed comparing fasted and fed groups of the two genotypes: fasted n=6, fed n=8. Statistical analysis for (C-I) ANOVA contrasts, \*p<0.05, \*\*p<0.01, \*\*\*p<0.0001.

# Figure S7

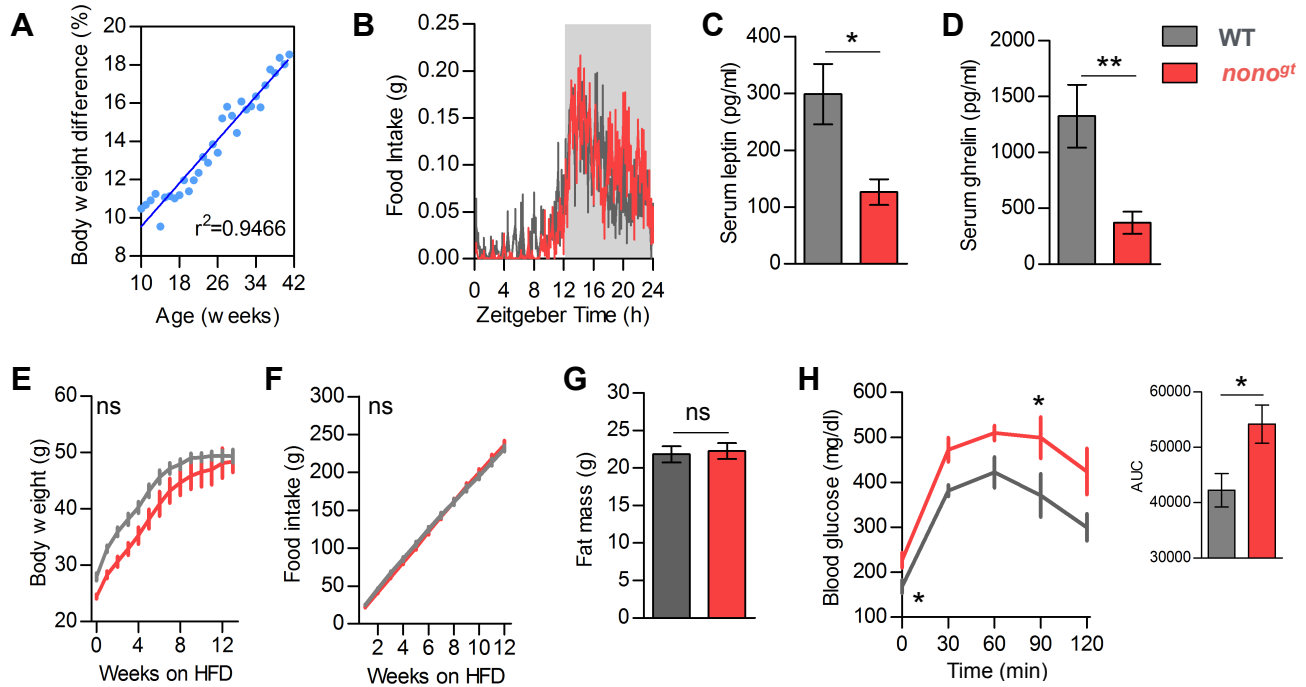


**Figure S7. An high fat diet can compensate for defective glucose uptake and storage in *nono<sup>gt</sup>* mice. Related to Figure 6.**

(A) Percent body weight difference between *wt* and *nono<sup>gt</sup>* mice from 10 to 42 weeks of age. When mice are on normal chow the body weight difference increases linearly with age ( $r^2=0.9466$ ). (B) Food intake during 24 h (15 minutes bin) average of 4 consecutive days,  $n=4$  per group. (C) Serum leptin levels after 12h of light-phase fasting, WT  $n=6$ , *nono<sup>gt</sup>*  $n=6$ . (D) Serum ghrelin levels after 12h of light-phase fasting, WT  $n=8$ , *nono<sup>gt</sup>*  $n=8$ . (E) Body weight curve during 12 weeks of HFD. (F) Cumulative food consumption of the same mice as in (E). (G) Fat mass of the same mice after 12 weeks on high fat diet. (H) Glucose tolerance test after 12 weeks on high fat diet, glucose (1g/kg), right panel AUC. For panels E-H WT  $n=6$ , *nono<sup>gt</sup>*  $n=5$ . Results are represented as mean $\pm$ SEM. Statistical analysis for (E), (F) and (H) 2-way ANOVA, Bonferroni posttest. In (H) on the bottom left of the panel is indicated the ANOVA p value for difference between genotypes. Statistical analysis for (C), (D), (G) and AUC student t test. \* $p<0.05$ , \*\* $p<0.01$ .